INFLUENCE OF THE MAGNITUDE AND DIRECTION OF DC-INJECTION CURRENT ON SPIN ACCUMULATION AND THERMOEMF IN NiCo-InSb-NiCo LATERAL SPIN VALVE

Yuriy V. Nikulin, Mikhail E. Seleznev, Alexander G. Veselov, Yuriy A. Filimonov

Kotelnikov Institute of Radioengineering and Electronics of RAS, Saratov Branch, http://www.cplire.ru/rus/sfire
39, Zelenaya str., Saratov 410019, Russian Federation

yvnikulin@gmail.com, mixanich94@mail.ru, labsftwo@mail.ru, yuri.a.filimonov@gmail.com

Abstract. **The influence of the direction and magnitude of the dc-injection current I (5μA-2 mA) on the spin accumulation U_s and the thermo electromotive force U_e in the NiCo-InSb-NiCo lateral spin-valve structure based on textured n-InSb(111) film with thickness d ≈ 500 nm and an electron mobility μH ≈ 2.1 m²/V·s were studied. For non-local injection and detection geometry at T ≈ 300 K it was found that at injection current I less than critical Ic, the value of which is determined by the geometry of the structure, the detected voltage $U_{ac} = U_s + U_e$ increases linearly with I from units to a few hundred microvolts and differs in sign for direct and reverse directions of injection current ($|I| < I_c$ is the region of spin accumulation, $U_{ac} \approx U_s$). At injection currents $|I| > I_c$, a sharp increase of the detected voltage to a few units or tens of millivolts is observed, and the sign of the detected voltage is positive for both directions of the injection current (at $|I| > I_c$ dominates the thermoe-lectric effect, $U_{ac} \approx U_e$, $U_s << U_e$).**

Keywords: **lateral spin valve, semiconductors indium-antimonide, ferromagnetic metals, spin transport**

PACS: 72.25.-b, 73.40.-c

Bibliography - 41 references *Received 12 November 2018; accepted 10 December 2018*

RENSIT, 2018, 10(3):373-380 **DOI: 10.17725/rensit.2018.10.373**

Contents

1. **Introduction (373)**
2. **Materials and Methods (375)**
3. **Results and Discussion (376)**
4. **Conclusion (378)**

References (378)

1. INTRODUCTION

Investigation of the spin-transport phenomena in micro- and nanostructures is of interest due to the possibility of development and optimization of spintronic devices – hard disk, MRAM devices, high sensitive microwave detectors, spin transistor and biosensor [1-9]. Nowdays, multilayer spin-valve structures with vertical arrangement of the injection and detection ferromagnetic electrodes (FM) separated by a thin layer of a paramagnetic metal or insulator are applied as an "active" element in the majority of spintronic devices [10]. However, there is a growing interest to investigation of spin-valve structures with lateral geometry of injection and detection FM electrodes connected by a "bridge" of paramagnetic metal [11-25], semiconductor [26-32], graphen [33, 34] or conducting polymer material [35]. This location of FM electrodes in a lateral spin-valve structure (LSV) gives it possible to separate injection's circuit of spin-polarized current and detection's circuit by means of a non-local geometry of spin injection and accumulation proposed in [36]. The advantage of the non-local geometry is a possibility to generate and detect "pure" spin current – diffusion current of electrons not associated with a charge transfer. Besides, "pure" spin current in LSV can be controlled by changing the magnetization direction of the injection and detection FM electrodes from parallel direction to antiparallel as in vertical spin valves.

The main physical parameters of materials applied for creation FM and NM electrodes in LSV structure are spin polarization of electrons in FM metal, spin diffusion length of electrons in

non-magnetic (NM) material and cleanliness of interface between FM metal and NM material. Thus, to increase the spin accumulation voltage, strong ferromagnetic materials with high spin polarization like NiFe [12-19, 21, 22, 32, 33, 35], FeCo [25], Co [14, 15, 23, 30, 34], CoFeAl [11, 18], Co_2FeSi [20, 24, 31] and nonmagnetic materials with the highest spin diffusion length [11-34] are applied to form FM and NM electrodes.

Currently, LSV structures based on polycrystalline films of ferromagnetic and paramagnetic metals Cu [13-25], Al [14, 25], Ag [12, 17, 25], Au [15, 25] got the most widespread due to simplicity of fabrication such structures. However, spin diffusion length of paramagnetic metals commonly less than few hundreds nanometers [11-25, 37]. By this reason, the magnitude of spin accumulation voltage U_s measured in non-local geometry for FM-NM metal based LSV structures is of few microvolts magnitude at cryogenic temperature [11-25]. Note, that U_s for such LSV can be increased to few hundreds microvolts at cryogenic temperatures by using the tunnel barrier between FM and NM metals [12-25].

It should be expected that U_s can be significantly increased at room temperature if spin transmitting channel is made of material with much higher λ_s and μ than that of paramagnetic metals. By this reason, semiconductors and graphen are the most perspective materials. LSV structures based on monocrystalline InAs, GaAs, InSb and graphen were discussed in [26-34]. Spin diffusion length was estimated to be $\lambda_s \approx 1.5\text{-}4$ μm for LSV structures based on graphen [33, 34], $\lambda_s \approx 1.9$ μm for InAs [30], $\lambda_s \approx 6.2$ μm for GaAs [31] and $\lambda_s \approx 25$ μm for monocrystalline *n*-InSb [26, 27]. The highest value of the spin diffusion length for monocrystalline InSb is due to the highest electron mobility in *n*-InSb ($\mu H \approx 6$ m^2/V·s at 300 K and 70 m^2/V·s at 77 K) in comparison with other semiconductors [38].

Taking to account potential advantages of epitaxial InSb films for creation a spin channel in LSV structure, needs to note, that the requirement of the small lattice mismatch between film and substrate imposes severe restrictions on the choice of a substrate material for growth of epitaxial InSb film and as a result complicates the technology of fabrication LSV structures. So, development of LSV structures with spin transmitting channel produced from polycrystalline InSb films with high electron mobility is of great practical interest. Due to the fact, that polycrystalline films can be grown on any nonorientating substrates, for example, glass, silicon oxide, polycor, this possibility can significantly increase a range of application of ferromagnetic metal – semiconductor based LSV structures. However, LSV structures with spin transmitting channel made of a polycrystalline InSb film until now has not been discussed [11-34].

This work shows, that LSV structure with distance between FM electrodes w ≈ 1.5 μm and spin transmitting channel prepared from textured *n*-InSb(111) film with electron mobility 2.1 m^2/V·s at 300 K can effectively accumulate spin voltage U_s up to few hundreds microvolts at room temperature. The influence of the magnitude and direction of the injected dc-current on spin accumulation voltage U_s and thermoEMF U_e in non-local geometry of injection and detection at room temperature is discussed.

2. MATERIALS AND METHODS

Lateral spin-valve structure NiCo($d \approx 30$ nm)/InSb($d \approx 500$ nm)/NiCo($d \approx 30$ nm) was produced by dc-magnetron sputtering (NiCo), thermal evaporation (InSb), positive photolithography and ion etching on polycor substrate (**Fig. 1**a). At the first step, InSb film with thickness $d \approx 500$ nm (Dektak 150, Veeco) was formed on a polycor substrate by thermal impulse evaporation [39]. XRD analysis (DRON-8, "Burevestnik") shows that InSb film has a strong (111) texture with texture coefficient k ≈ 0.016, i.e. 98.4% of crystallites are oriented in [111] direction perpendicular to the substrate

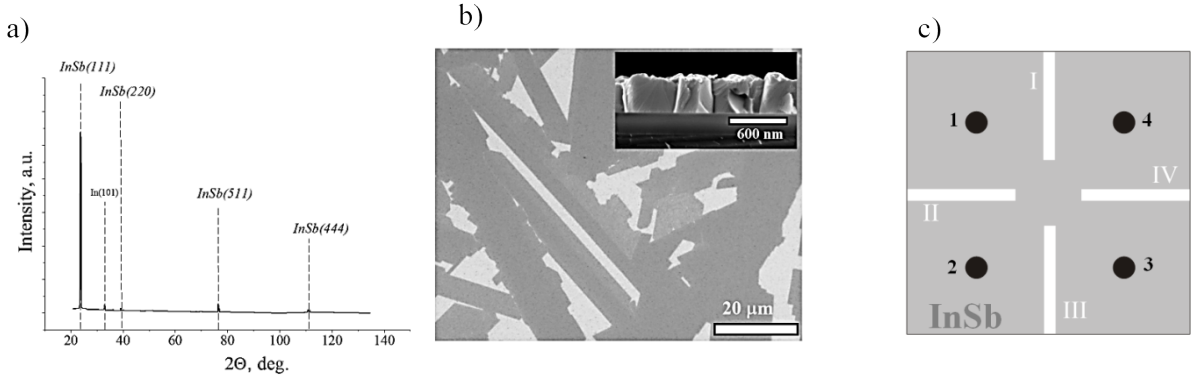

Fig. 1. *(a) X-ray diffraction pattern of n-InSb(111) film with thickness 500 nm; (b) optical picture of the surface of n-InSb(111) film. The inset of the picture (b) shows the cross section image of InSb film with thickness d ≈ 600 nm; (c) schematic image of a sample formed from InSb film on a polycor substrate (10×10 mm²) for Van Der Pauw measurements.*

surface (Fig. 1a). Mass concentrations of the crystal phases correspond InSb-97%, In-2%, In_2O_3 – 1%. The content of the amorphous phase in the film is about 0.4-2%. The average size of the coherent scattering region is 250 nm. According to data of optical (Olympus, MX-4) and scanning electronic (Auriga, Carl Zeiss) microscopies InSb film possesses a mosaic surface morphology and column microstructure (Fig. 1a).

Estimations of the electron mobility μ_H [$m^2/V{\cdot}s$], Hall coefficient R_H [m^3/C], resistivity ϱ [Ohm·m] and charge carrier concentration n [m^{-3}] for InSb film were carried out by the Van Der Pauw technique [40, 41] at room temperature in magnetic field (B ≈ 0.2 **T**) applied perpendicular to surface of InSb film. Fig. 1 shows a schematic image of the measured InSb sample. Digits 1-4 denote conducting point contacts, I-IV – deleted parts of InSb film.

Estimations of μ_H, R_H, ϱ and n were carried out according to [41]:

$$\rho \approx \frac{\pi d}{\ln 2}\left(\frac{R_{12,34}+R_{23,41}}{2}\right)\left(1-\frac{\ln 2}{2}\left(\frac{R_{12,34}-R_{23,41}}{R_{12,34}+R_{23,41}}\right)\right), \quad (1)$$

$$R_H \approx \frac{\Delta U_{24} d}{I_{24} B}, \quad (2)$$

$$\mu_H \approx \frac{R_H}{\rho}, \quad (3)$$

$$n \approx \frac{1}{eR_H}, \quad (4)$$

where d is a thickness of the InSb film, $R_{12,34} \approx \frac{U_{34}}{I_{12}}$ is a relation of voltage, measured between contacts 3 – 4 to current I between contacts 1–2; $R_{23,41} \approx \frac{U_{41}}{I_{23}}$ – is a relation of voltage, measured between contacts 4–1 to current I between contacts 2–3; ΔU_{24} is a voltage change of U_{24} caused by a magnetic field $B \approx 0.2$ T; $e \approx 1.602 \cdot 10^{-19}$ C – charge of electron.

As a result of the measurement, following estimates of μ_H, R_H, ϱ and n of textured n-InSb(111) film with thickness 500 nm were obtained: $\mu_H \approx 2.1$ $m^2/V{\cdot}s$, $R_H \approx 1.06 \cdot 10^{-4}$ m^3/C, $\varrho \approx 49 \cdot 10^{-6}$ Ohm·m and $n \approx 5.8 \cdot 10^{22}$ m^{-3}.

At the second step, the pattern of contacts and spin channel of width $w \approx 1.5$ μm (**Fig. 2***a*) was formed on the surface of the InSb film by a positive photolithography and ion etching. In the third step, NiCo film with thickness $d \approx 30$ nm was dc-sputtered on the surface of the InSb film. Next, ferromagnetic injector and detector electrodes with width $w \approx 1.5$ μm and distance between each other $w \approx 1.5$ μm were formed on the surface of the NiCo film by positive photolithography and ion etching (Fig. 2b).

To verify contact impedance of the indium antimonide–NiCo contact volt-ampere characteristic (VAC) was measured in the current range $|I| \leq 2$ mA. Cruciform structure, consisting of two intersecting microstrips of InSb ($d \approx 500$ nm) and NiCo ($d \approx 30$ nm) with width $w \approx 1.5$ μm was prepared for VAC measurements. Results of the VAC measurements of the InSb-NiCo

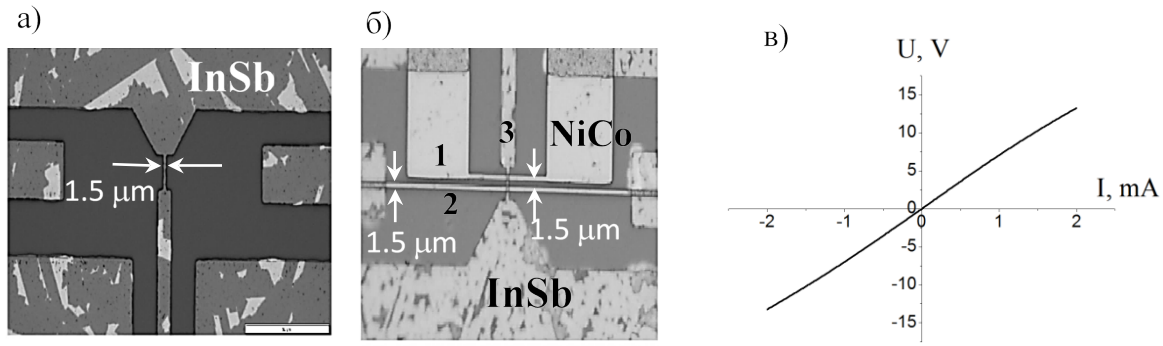

Fig. 2. *(a) System of InSb electrodes with width of the spin transmitting channel w ≈ 1.5 μm; (b) System of NiCo(1,2) electrodes with width w ≈ 1.5 μm and located over the top of the InSb electrodes (3). Distance between FM electrodes is w ≈ 1.5 μm; (c) VAC characteristic of the contact InSb-NiCo measured in currents range |I| ≤ 2 mA.*

contact show that this structure possesses non-rectifying contact in the ferromagnetic metal-indium antimonide interface. As follows from the Fig. 2*c*, VAC is close to linear at $|I| \leq 1.5$ mA and there is a small nonlinearity at $|I| \geq 1.5$ mA of the contact, which may be caused by a thin layer of In_2O_3 between InSb and NiCo films formed during deposition of InSb film.

3. RESULTS AND DISCUSSIONS

Current's measurements in LSV structure were performed in non-local geometry of spin injection and detection at room temperature by a four probe technique. **Fig. 3**a shows a scheme of the measurements. Direct current I with magnitude $I \approx 1$ μA–1.2 mA was injected to the structure in two directions I^+ и I^- at $T \approx 300$ K. Magnetic field $H \approx \pm 0.3$ kOe was applied parallel to FM electrodes. This range of H corresponds to the field where each ferromagnetic electrode shows magnetoresistive effect. For each definite magnitude and direction of the injected current I were determined dependences of the resistance R of the detecting contact on the magnetic field H magnitude, where $R = U_{ac}/I$, $U_{ac} = U_s + U_e$, U_{ac} – detecting voltage, I – current injected to the structure, U_s – voltage of the spin accumulation, U_e – voltage of the thermoelectric effect (Fig. 3b). Values of R_{ap}, R_p, $\angle R = R_{ap} - R_p$ and $U_{ac} = \Delta R \cdot |I|$ were determined from $R(H)$ dependences, where R_{ap} – resistance of the structure, when directions of the magnetizations of detector and injector FM electrodes are closer to anti-parallel, R_p – resistance of the structure in magnetic field H corresponding to saturation field of FM electrodes.

Dependences R_{ap}, ΔR and $U_{ac} = \Delta R \cdot |I|$ on the magnitude and direction of injected current I at T ≈ 300 K are shown in the **Fig. 4***a-c*. As can be seen, values R_{ap} and ΔR don't depend on I at I less than critical current I_c ($I < I_{c+} \approx 1.1$ mA and $I < I_{c-} \approx 0.5$ mA), but U_{ac} increases linearly with I up to $|U_{ac}| \approx 250$–500 μV. It is known that magnitude of the spin voltage U_s depends on the injecting current I linearly [27]:

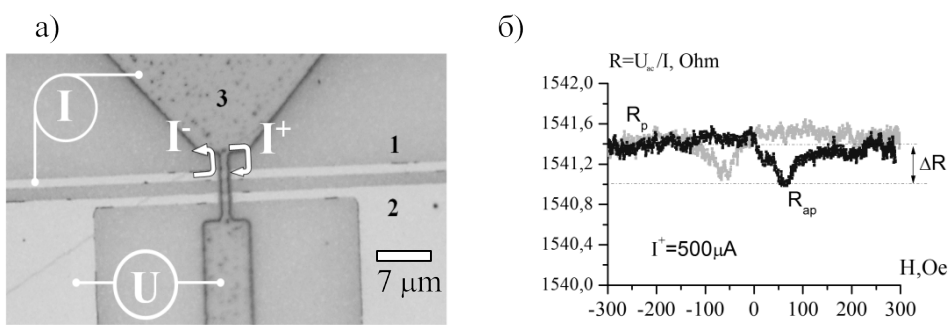

Fig. 3. *(a) Non-local geometry of spin injection and detection for lateral spin-valve structure NiCo-InSb-NiCo. Ferromagnetic electrodes marked as 1 and 2; InSb channel marked as 3; (b) Dependence of parameter R on external field H for injection current I ≈ 500 μA, where R = U_{ac}/I, U_{ac} – measured voltage, I – injection current.*

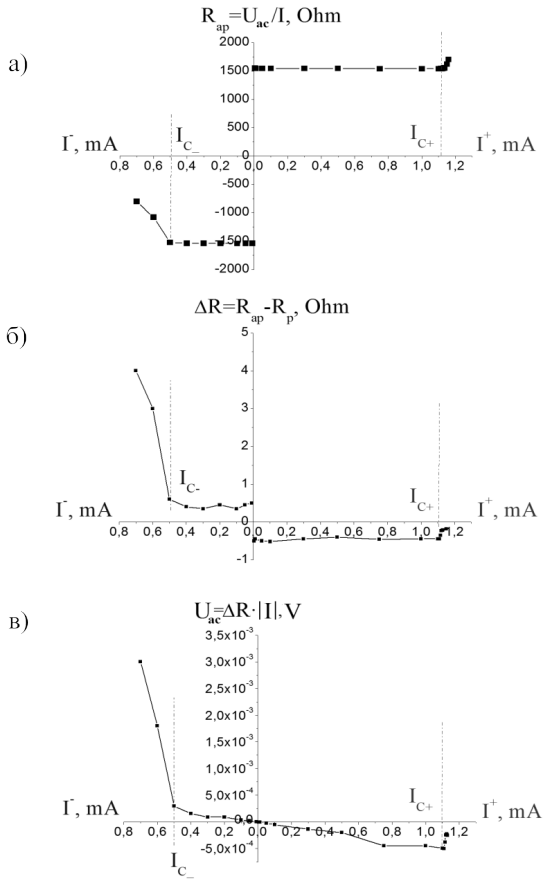

Fig. 4. *Dependences of parameters (a) R_{ap}, (b) $\Delta R = R_{ap} - R_p$ and (c) $U_{ac} = \Delta R \cdot |I|$ on a magnitude and direction of current I injected to the structure at room temperature.*

$$U_s = \frac{P^2 I \lambda_s \rho}{2A} e^{-\frac{w}{\lambda_s}}, \quad (5)$$

where I – injecting current, w – distance between ferromagnetic electrodes, λ_s – spin diffusion length in nonmagnetic material, P – electron polarization near the nonmagnetic material interface, ρ – resistivity of nonmagnetic material, A – cross-sectional area of the spin transmitting channel.

Therefore, we could conclude that the range of injection currents $|I| < I_c$ corresponds to the range in which spin accumulation voltage U_s dominates in the measured voltage U_{ac}, $U_{ac} \approx U_s$, $U_e \approx 0$.

It should note that the value of the critical current is substantially determined by a geometry and shapes of electrodes of the spin-valve structures, by thickness of the ferromagnetic and nonmagnetic films and, in general, by the technology of producing LSV structure. In our case, difference between I_{c+} и I_{c-} can be explained by a shape asymmetry of FM and InSb electrodes and area difference of FM and InSb electrodes.

At injection currents higher than critical value I_c ($I > I_{c+} \approx 1.1$ mA and $I > I_{c-} \approx 0.5$ mA) there is a sharp increase of the detectable voltage U_{ac} for one direction of the injection current ("negative" I_{c-}) and a change of the sign of the $U_{ac}(I)$ dependence for reverse ("positive" I_{c+}) direction of I. Such behavior of $U_{ac}(I)$ dependence can be caused by contribution of thermoEMF U_e to the voltage U_{ac} due to the resistive heating of the LSV structure at large injection currents [14]. When injected current flows through the contact of indium antimonide – ferromagnetic metal, independently on the current's direction, it causes a Joule heating. So, we can assume that the second detection contact play a role of a thermocouple, for which heating is always accompanied by generation of thermEMF of positive polarity. Thus, it can be concluded, that a range of currents $|I| > I_c$ correspond to the range where thermoEMF dominates in detectable voltage U_{ac}, i.e. $U_{ac} \approx U_e$, $U_s << U_e$.

4. CONCLUSION

Influence of the direction and magnitude of injection current I (5 μA–2 mA) on the spin accumulation voltage in the lateral spin-valve structure ferromagnetic metal (NiCo) – indium antimonide with spin transmitting channel formed of a texture film InSb (111) with electron mobility 2.1 $m^2/V \cdot s$ was investigated. For non-local geometry of the injection and detection at $T \approx 300$ K were determined current dependences of parameters R_{ap}, $\Delta R = R_p - R_{ap}$ и $U_{ac} = \Delta R \cdot I$, where U_s – spin accumulation voltage, U_e – voltage of a thermoelectric effect, R_{ap} resistance of the structure at "quasi" antiparallel direction of the magnetizations of the detection and injection ferromagnetic (FM) electrodes, R_p – resistance of LSV structure in the saturation magnetic field H corresponding to the parallel magnetization of FM electrodes.

It was established that at $T \approx 300$ K and injection currents I less than critical I_c which magnitude is determined by a geometry of the LSV structure, the magnitude of R_{ap} and ΔR, almost independent on I, but U_{ac} linearly increase with current from units to few hundreds microvolts (the range of spin accumulation, $U_{ac} \approx U_s$). At injection currents $|I| > I_c$ there are a sharp increase in magnitude of ΔR and U_{ac} for one current's direction and sign change of $\Delta R(I)$ and $U_{ac}(I)$ dependences for other current's direction due to resistive heating of the structure at large injection current ($|I| > I_c$ – the currents range, where thermoelectric effect dominates, $U_{ac} \approx U_e$, $U_s << U_e$).

Obtained results could be of interest at creation high sensitive microwave detectors based on the lateral spin-valve ferromagnetic metal-indium antimonide structures [17].

ACKNOWLEDGMENTS

This work was supported by RFBR, projects № 16-37-60052, 16-29-14058.

REFERENCES

1. Fang B, Carpentieri M, Hao X, Jiang H, Katine JA, Krivorotov IN, Ocker B, Langer J, Wang KL, Zhang B, Azzerboni B, Amiri PK, Finocchio G, Zeng Z. Giant spin-torque diode sensitivity in the absence of bias magnetic field. *Nature Commutications,* 2016, 7(11259):1-7.
2. Gui YS., Xiao Y, Bai LH, Hemour S, Zhao Y P, Houssameddine D, Wu K, Guo H, Hu CM. High sensitivity microwave detection using a magnetic tunnel junction in the absence of an external applied magnetic field. *Appl. Phys. Lett.*, 2015, 106 (152403):1-6.
3. Fan X, Cao R, Moriyama T, Wang W, Zhang HW, Xiao JQ. Magnetic tunnel junction based microwave detector. *Appl. Phys. Lett.*, 2009, 122501:1-4.
4. Li X., Zhou Y, Zheng C, Chan PH., Chan M, Pong PWT. Field–angle and DC-bias dependence of spin-torque diode in giant magnetoresistive Microstripe. *Appl. Phys. Lett.*, 2016, 109 (192402):1–6.
5. Kumar PSA, Lodder JC. The spin-valve transistor. *J. Phys. D: Appl. Phys.*, 2000, 33:2911-2920.
6. Fu L, Gui YS, Bai LH, Guo H, Abou-Rachid H, Hu CM. Microwave holography using a magnetic tunnel junction based spintronic microwave Sensor. *J. Appl. Phys.*, 2015, 117 (213902):1-6.
7. Tulapurkar AA, Suzuki A, Fukushima A, Kubota H, Maehara H, Tsunekawa K, Djayaprawira DD, Watanabe N, Yuasa S. Spin-torque diode effect in magnetic tunnel junctions. *Nature*, 2005, 438:339-342.
8. Deen DA, Pokhil TG, Singleton E, Patwari MSU. Lateral spin valve reader with large–area tunneling spin injector. US Patent, № US9685178B1, 20 June 2017.
9. Hall DA, Gaster RS, Lin T, Osterfeld SJ, Han S, Murmann B, Wang SX. GMR biosensor arrays:A system perspective. *Biosensors and Bioelectronics*, 2010, 25(9):2051-2057.
10. Wu Y. *Nano Spintronics for Data Storage. Encyclopedia of Nanoscience and Nanotechnology*, Edited by H.S. Nalwa, Stevenson Ranch, Calif., 2004, 10:1-50.
11. Hu S, Nomura T, Uematsu G, Asam N, Kimura T. First- and second-harmonic detection of spin accumulation in a multiterminal lateral spin valve under high-bias ac current. *Phys. Rev. B.*, 2016, 94(014416):1-5.
12. Fukuma Y, Wang L, Idzuchi H, Takahashi S, Maekawa S, Otani YC. Giant enhancement of spin accumulation and long–distance spin precession in metallic lateral spin valves. **Nature Materials**, 2011, 10:527-531.
13. Otani Y, Kimura T. Manipulation of spin currents in metallic Systems. *Phil. Trans. R. Soc. A.*, 2011, 369:3136-3149.
14. Casanova F, Sharoni A, Erekhinsky M, Schuller IK. Control of spin injection by direct current in lateral spin valves. *Phys. Rev. B.*, 2009, 79(184415):1-6.

15. Ji Y, Hoffmann A, Jiang JS, Pearson JE, Bader SD. Non-local spin injection in lateral spin valves. *J. Phys. D: Appl. Phys.*, 2007, 40:1280-1284.
16. Kimura T, Hamrle J, OtaniY, Tsukagoshi K, Aoyagi Y. Spin-dependent boundary resistance in the lateral spin–valve structure. *Appl. Phys. Letters*, 2004, 85:3501-3503.
17. Kuhlmann N, Swoboda C, Vogel A, Matsuyama T, Meier G. All-metal lateral spin valve operated by spin pumping. *Phys. Rev. B.*, 2013, 87(104409):1-5.
18. Nomura T, Ohnishi K, Kimura T. Large spin current injection in nano-pillar-based lateral spin valve. *AIP Conference Proceedings*, 2016, 1763(020011):1-5.
19. Nonoguchi S, Nomura T, Kimura T. Longitudinal and transverse spin current absorptions in a lateral spin-valve structure. *Phys. Rev. B.*, 2012, 86(104417):1-5.
20. Oki S, Kurokawa T, Honda S, Yamada S, Kanashima T, Itoh H, Hamaya K. Robust spin-current injection in lateral spin valves with two-terminal Co_2FeSi spin Injectors. *AIP Advances*, 2017, 7(055808):1-7.
21. Erekhinsky M, Sharoni A, Casanova F, Schuller IK. Surface enhanced spin-flip scattering in lateral spin valves. *Appl. Phys. Lett.*, 2010, 96(022513):1-3.
22. Kimura T, Hamrle J, Otani Y. Estimation of spin-diffusion length from the magnitude of spin–current absorption: Multiterminal ferromagnetic/nonferromagnetic hybrid structures. *Phys. Rev. B.*, 2005, 72(014461):1-6.
23. Smith AK, Jamali M, Stecklein G, Crowell PA, Wang JP. Demonstration of nonlocal lateral spin valve devices fabricated with a versatile top-down fabrication process. *IEEE Magnetics Lett.*, 2015, 6:1-5.
24. Yamasaki K, Oki S, Yamada S, Kanashima T, Hamaya K. Spin-related thermoelectric conversion in lateral spin-valve deviceswith single–crystalline Co_2FeSi electrodes. *Appl. Phys. Express*, 2015, 8(043003):1-4.
25. Idzuchi H, Fukuma Y, Otani YC. Spin transport in non-magnetic nanostructures induced by non-local spin injection. *Physica E*, 2015, 68:239-263.
26. Viglin NA, Ustinov VV, Demokritov SO, Shorikov AO, Bebenin NG, Tsvelikhovskaya VM, Pavlov TN, Patrakov EI. Electric measurement and magnetic control of spin transport in InSb-based lateral spin devices. *Phys. Rev. B*, 2017, 96(235303):1-10.
27. Viglin NA, Ustinov VV, Tsvelikhovskaya VM, Pavlov TN. Electric Injection and Detection of Spin-Polarized Electrons in Lateral Spin Valves on Ferromagnetic Metal-Semiconductor InSb Heterojunctions. *JETP Letters,* 2015, 101(2):113-117.
28. Kim YJ. Electrical injection and detection of spin polarization in InSb/ferromagnet nanostructures. *PhD Thesis*, 2012, Blacksburg, Virginia.
29. Saha D, Holub M, Bhattacharya P, Liao YC. Epitaxially grown MnAs/GaAs lateral spin valves. *Appl. Phys. Lett.*, 2006, 89(142504):1-3.
30. Wang Z, Pan D, Wang L, Wang T, Zhao B, Wu Y, Yang M, Xu X, Miao J, Zhao J, Jiang Y. Room temperature spin transport in InAs nanowire lateral spin valve. *RSC Adv.*, 2016, 6(79):75736-75740.
31. Bruski P, Manzke Y, Farshchi R, Brandt O, Herfort J, Ramsteiner M. All-electrical spin injection and detection in the Co_2FeSi/GaAs hybrid system in the local and non-local configuration. *Appl. Phys. Lett.*, 2013, 103(052406):1-5.
32. Last T, Wahle M, Hacia S, Fischer SF, Kunze U. Local Hall Effect and Ballistic Transport in Multi-terminal InAs-Based Lateral Spin-Valve Tunnelling Devices. *J. Superconductivity: Incorporating Novel Magnetism*, 2005, 18(3):385-389.
33. Lin CC, Penumatcha AV, Gao Y, Diep VQ, Appenzeller J, Chen Z. Spin Transfer Torque in a Graphene Lateral Spin Valve Assisted by an External Magnetic Field. *Nanoletters,* 2013, 13(11):5177-5181.

34. Tombros N, Jozsa C, Popinciuc M, Jonkman HT, van Wees BJ. Electronic spin transport and spin precession in single graphene layers at room temperature. *Nature*, 2007, 448:571-575.
35. Kawasugi Y, Ara M, Ushirokita H, Kamiya T, Tada H. Preparation of lateral spin-valve structure using doped conducting polymer poly(3,4-ethylenedioxythiophene) poly(styrenesulfonate). *Organic Electronics*, 2013, 14:1869-1873.
36. Johnson M, Silsbee RH. Interfacial charge-spin coupling: Injection and detection of spin magnetization in metals. *Phys. Rev. Lett.*, 1985, 55(17):1790-1793.
37. Coey JMD. *Magnetism and magnetic materials.* New York, Cambridge university press, 2010, 633 p.
38. Sluchinskaya IA. *Osnovy materialovedeniya i techniki poluprovodnikov* [Base principals of the semiconductors material science and industry]. Moscow, Mir Publ., 2002, 376 p.
39. Gulyaev YV, Veselov AA, Veselov AG, Buriylin EI, Dzhumaliev AS, Zyuryukin YA, Kiryasova OA, Ryabushkin SL. *ZhTF*, 2004, 74(8):113-115.
40. Van der Pauw LJ. A method of measuring the resistivity and Hall coefficient on lamellae of arbitrary shape. *Philips Tech. Rev.*, 1958, 20(8):220-224.
41. Kuchis EV *Galvanomagnitniye effektiy i metody ih issledovaniya* [Galvanomagnetic effects and methods of investigations]. Moscow, Radio i Svyaz Publ., 1990, 264 p.